Journal of Computational Physics 229 (2010) 7672–7691

Contents lists available at ScienceDirect

Journal of Computational Physics

journal homepage: www.elsevier.com/locate/jcp

Numerical study of a stochastic particle algorithm solving a multidimensional population balance model for high shear granulation

Andreas Braumann [a], Markus Kraft [a,*], Wolfgang Wagner [b]

[a] Department of Chemical Engineering and Biotechnology, University of Cambridge, Pembroke Street, Cambridge CB2 3RA, United Kingdom
[b] Weierstrass Institute for Applied Analysis and Stochastics, Mohrenstraße 39, 10117 Berlin, Germany

ARTICLE INFO

Article history:
Received 16 February 2010
Received in revised form 9 June 2010
Accepted 10 June 2010
Available online 18 June 2010

Keywords:
Granulation
Population balance
Direct Simulation Monte Carlo

ABSTRACT

This paper is concerned with computational aspects of a multidimensional population balance model of a wet granulation process. Wet granulation is a manufacturing method to form composite particles, granules, from small particles and binders. A detailed numerical study of a stochastic particle algorithm for the solution of a five-dimensional population balance model for wet granulation is presented. Each particle consists of two types of solids (containing pores) and of external and internal liquid (located in the pores). Several transformations of particles are considered, including coalescence, compaction and breakage. A convergence study is performed with respect to the parameter that determines the number of numerical particles. Averaged properties of the system are computed. In addition, the ensemble is subdivided into practically relevant size classes and analysed with respect to the amount of mass and the particle porosity in each class. These results illustrate the importance of the multidimensional approach. Finally, the kinetic equation corresponding to the stochastic model is discussed.

1. Introduction

This paper is concerned with computational aspects of a multidimensional population balance model of a wet granulation process. Wet granulation is a manufacturing method to form composite particles, granules, from small particles and binders, using equipment such as rotating drums, fluidised beds and high-shear mixers [1]. These composites have enhanced handling properties over their raw components, and are used for a variety of products, ranging from fertilizers to drugs and detergents. In order to yield granules with a high product quality, a good understanding of the process is required, which may be obtained through modelling of the granulation process. The formation of granules can be described with population balances models, allowing the tracking of the number of particles with desired properties.

Since the 1960s one-dimensional population balance models, i.e., with one characteristic property, have been used to describe granulation processes [2,3]. A one-dimensional description of the granules was subsequently found to be insufficient [4,5], and models with three or more dimensions have been introduced [6–10]. Several approaches have been applied for the numerical solution of population balance models. These are for instance the method of moments [11], sectional methods [12–15], and finite element methods [16]. However, the computational effort for the solution of the models with these methods increases enormously, if the number of dimensions is changed from one to two, three, or even more. Stochastic particle methods offer an attractive alternative for the solution of multidimensional population balance models and have successfully been applied to granulation models [9,10]. Moreover, stochastic algorithms have not only been applied to models

* Corresponding author. Tel.: +44 1223 762784; fax: +44 1223 334796.
E-mail address: mk306@cam.ac.uk (M. Kraft).

0021-9991/$ - see front matter © 2010 Elsevier Inc. All rights reserved.
doi:10.1016/j.jcp.2010.06.021

for particulate processes such as crystallisation [17], nanoparticle synthesis [18–22] and granulation [23,24], but also to those for chemical reactions [25], liquid–liquid mixing [26,27] and droplet coalescence in clouds [28]. Several studies investigated the stochastic treatment of aggregation processes for one- and two-dimensional models [29–33]. Despite this wealth of studies, it remains open how stochastic algorithms would perform for a model with a higher number of dimensions and additional processes, for instance breakage of particles. In addition, an assessment of the numerical approach with respect to the numerical errors is important, in particular, when the solutions for different models are computed in order to discriminate one over the other model. Another aspect in model development is the solving of the inverse problem, i.e., the estimation of model parameters using experimental observations. A detailed understanding of the numerical solution of complex, multivariate models is beneficial, given that surrogate models may be constructed and used for this task.

The purpose of this paper is to present a detailed numerical study of a stochastic particle algorithm for the solution of a five-dimensional population balance model for wet granulation. In particular, the influence of numerical parameters on the macroscopic properties of the particle ensemble is investigated.

A description of the stochastic particle model is given in Section 2. Each particle consists of two types of solids (containing pores) and of external and internal liquid (located in the pores). Several transformations are introduced that correspond to coalescence, compaction and breakage of particles. Numerical results are presented in Section 3. A convergence study is performed with respect to the parameter which determines the number of particles in the system. Several interesting properties of the system are computed, like the number of particles per unit volume and the mean particle porosity. In addition, the ensemble is subdivided into practically relevant size classes and analysed with respect to the amount of mass and the particle porosity in each class. These results illustrate the importance of the multidimensional approach. Finally, in Appendix A, the kinetic equation corresponding to the stochastic model studied in this paper is discussed.

2. Model

The mathematical model is a jump process characterised by the state space, the jump rates and the jump transformations. Its purpose is to describe the evolution of particles in a high shear granulation process. The particle vector

$$x = (s_o, s_r, l_e, l_i, p)$$

consists of non-negative internal variables, which are

- original solid volume s_o,
- reacted solid volume s_r,
- external liquid volume l_e,
- internal liquid volume l_i and
- pore volume p.

Note that

$$l_i \leqslant p \quad \text{and} \quad s_o + s_r = 0 \Rightarrow p = 0. \tag{1}$$

Several dependent variables are defined. The particle volume is

$$v(x) = s_o + s_r + l_e + p. \tag{2}$$

The particle radius is (assuming a spherical shape)

$$R(x) = \sqrt[3]{\frac{3}{4\pi} v(x)}.$$

With the assumption that the densities of the liquids and the reacted solid are the same,

$$\rho_{l_e} = \rho_{l_i} = \rho_{s_r}, \tag{3}$$

the particle mass takes the form

$$m(x) = \rho_{s_o} s_o + \rho_{l_e}(s_r + l_i + l_e),$$

where ρ_{s_o} and ρ_{l_e} are input parameters. The porosity is defined as

$$\varepsilon(x) = \frac{p}{v(x)}. \tag{4}$$

The external surface area is (spherical particle)

$$a_e(x) = \pi^{1/3}(6v(x))^{2/3}. \tag{5}$$

The internal surface area is

$$a_i(x) = Cp^{2/3} \quad \text{for some } C \geqslant 6^{2/3}\pi^{1/3} \approx 4.8.$$

The constant C is an input parameter, which has to be fitted. The higher the value of C is, the more tortuous are the pores. We use the value $C = 15$, which gave good results in [9].

The **initial state** of the system is a set of particles of the form

$$x = (s_o, 0, 0, 0, 0)$$

made up only of original solid. This set is composed according to a size distribution from experiments. Various processes are covered by the model:

1. **Addition of liquid**: Droplets of the form

$$x = (0, 0, l_e, 0, 0)$$

are added to the particle ensemble.
2. **Coagulation**: Two particles combine to a new particle. In addition to this, **compaction** takes place, i.e., the particle porosity is reduced.
3. **Breakage**: A particle splits into two particles.
4. **Processes within a particle** that do not change the number of particles in the ensemble:
   (a) **Chemical reaction**: Formation of the reaction product s_r.
   (b) **Penetration**: Migration of the external liquid l_e into the pores.

These processes are specified in the following.

2.1. Addition of liquid

Assuming that liquid addition is performed using a nozzle or similar device, two characteristic properties exist in order to describe the process:

- $\dot{V}_l$, the volumetric flow rate of the binder being added to the system, and
- $p^{in}(x)$, the number based normalised droplet size distribution that gives the probability that a droplet being added to the system is of type x.

Both are input parameters. The mean droplet size is given by

$$\overline{V}_{droplet} = \int_X v(x)p^{in}(x)dx,$$

where $X = [0,\infty)^5$ denotes the type space. The density rate of the "inflowing" particles is

$$f^{in}(x) = \frac{\dot{V}_l}{V_{reactor}} \frac{p^{in}(x)}{\overline{V}_{droplet}} \tag{6}$$

and the number inflow rate is

$$\int_X f^{in}(x)dx = \frac{\dot{V}_l}{V_{reactor}} \frac{1}{\overline{V}_{droplet}} \tag{7}$$

with $V_{reactor}$ being the volume where the particle ensemble is contained in.

In the special case of $p^{in}(x)$ being the delta function at

$$x = (0, 0, V_{droplet,mono}, 0, 0),$$

so that all droplets exhibit the same size, one obtains

$$\overline{V}_{droplet} = V_{droplet,mono}.$$

2.2. Collisions

The **collision rate** of particles with the properties x' and x'' is given by the kernel

$$K(x', x'') = n_{impeller}\widehat{K}_0 \tag{8}$$

with input parameters $n_{impeller}$ (impeller speed) and $\widehat{K}_0$ (rate constant).

The coalescence efficiency $\widetilde{K}$ is calculated based on the Stokes criterion, which is a function of the viscous Stokes number and the critical Stokes number, with

$$\widetilde{K}(x',x'') = \begin{cases} 1, & \text{if } e_{\text{coag}}(x',x'') = 0, \\ 1, & \text{if } e_{\text{coag}}(x',x'') > 0 \text{ and } \mathrm{St}_{\text{v}}^{*}(x',x'') \geqslant \mathrm{St}_{\text{v}}(x',x''), \\ 0, & \text{otherwise}. \end{cases}$$

The coefficient of restitution is defined as the geometric average of the coefficients of restitution of the single particles x' and x'',

$$e_{\text{coag}}(x',x'') = \sqrt{e(x') \cdot e(x'')}. \tag{9}$$

A mass-weighted arithmetic average is used for the calculation of the coefficient of restitution of each particle,

$$e(x) = \begin{cases} \frac{e_{s_o}\rho_{s_o}s_o + \rho_{l_e}(e_{s_r}s_r + e_{l_i}l_i)}{\rho_{s_o}s_o + \rho_{l_e}(s_r + l_i)}, & \text{if } s_o + s_r > 0, \\ 0, & \text{otherwise (droplet)}, \end{cases}$$

where $e_{s_o}, e_{s_r}, e_{l_i} \in [0,1]$ are input parameters.

The viscous Stokes number is computed as

$$\mathrm{St}_{\text{v}}(x',x'') = \frac{\tilde{m}(x',x'')U_{\text{col}}}{3\pi\eta\widetilde{R}(x',x'')^2},$$

with input parameters U_{col} (collision velocity) and η (binder viscosity). The harmonic mass of x' and x'' is

$$\tilde{m}(x',x'') = \frac{2m(x')m(x'')}{m(x') + m(x'')}.$$

The harmonic radius computes as

$$\widetilde{R}(x',x'') = \frac{2R(x')R(x'')}{R(x') + R(x'')}.$$

The critical Stokes number is defined by

$$\mathrm{St}_{\text{v}}^{*}(x',x'') = \left(1 + \frac{1}{e_{\text{coag}}(x',x'')}\right) \ln\left(\frac{h(x',x'')}{h_{\text{a}}}\right)$$

with the input parameter h_{a} (characteristic length scale of surface asperities). The thickness of the binder layer $h(x',x'')$ is defined as the combined binder thickness of the particles x' and x'',

$$h(x',x'') = \frac{h(x') + h(x'')}{2},$$

with the thickness of the binder layer of a particle with the properties x being calculated by

$$h(x) = \frac{1}{2}\sqrt[3]{\frac{6}{\pi}}\left[\sqrt[3]{v(x)} - \sqrt[3]{v(x) - l_{\text{e}}}\right].$$

The Stokes criterion was introduced by Ennis et al. [34] and measures whether the kinetic energy of a particle–particle collision can be dissipated by the viscous binder layer, so that the particles do not rebound. The Stokes number St_{v} is the ratio of the inertial to the viscous forces in a collision. The critical Stokes number $\mathrm{St}_{\text{v}}^{*}$ marks the upper limit of the Stokes numbers for which colliding particles do not rebound.

The **collision event** leads to the following outcomes:

- If $\widetilde{K}(x',x'') = 1$, then particles coalesce and are compacted, provided that no droplet is involved, i.e.,

  $$x', x'' \to T(x',x''),$$

  where

  $$T(x',x'') = \begin{cases} T_{+}(x',x''), & \text{if } x' \text{ or } x'' \text{ is a droplet}, \\ \widehat{T}(T_{+}(x',x'')), & \text{otherwise}. \end{cases}$$

- If $\widetilde{K}(x',x'') = 0$, then particles do not coalesce, but are compacted,

  $$x', x'' \to \widehat{T}(x'), \widehat{T}(x'').$$

The coalescence transformation T_{+} and the compaction transformation $\widehat{T}$ will be described in the subsections following below.

2.2.1. Coalescence transformation

If the particles

$$x' = (s'_o, s'_r, l'_e, l'_i, p'), \quad x'' = (s''_o, s''_r, l''_e, l''_i, p'')$$

coalesce, a new particle

$$x''' = (s'''_o, s'''_r, l'''_e, l'''_i, p''') =: T_+(x', x'')$$

arises. Its composition is defined in the following.

The volumes of the solid components are calculated as

$$s'''_o = s'_o + s''_o, \quad s'''_r = s'_r + s''_r.$$

Due to the coalescence event some external liquid is assumed to become trapped inside the new particle, i.e., the amount of internal liquid increases. This transferred volume of liquid $l_{e\to i}$ is computed by

$$l_{e\to i}(x', x'') = \left\{ l'_e l''_e \left[1 - \sqrt{1 - \left(\frac{\sqrt[3]{v(x')} - l'_e}{\sqrt[3]{v(x')} + \sqrt[3]{v(x'')}} \right)^2} \right] \times \left[1 - \sqrt{1 - \left(\frac{\sqrt[3]{v(x'')} - l''_e}{\sqrt[3]{v(x')} + \sqrt[3]{v(x'')}} \right)^2} \right] \right\}^{1/2}. \tag{10}$$

The volumes of the liquid components are calculated as

$$l'''_e = l'_e + l''_e - l_{e\to i}(x', x''), \quad l'''_i = l'_i + l''_i + l_{e\to i}(x', x'').$$

The pore volume p''' of the newly formed particle depends on the composition x' and x''. If these particles are rather "hard" it is assumed that the surface area of the new particle is equal to the combined surface area of the predecessors. In contrast to this, two "soft" particles will merge completely, so that their volumes add up to the volume of x'''. The "softness" of the particles is given by the coefficient of restitution (9). The pore volume is calculated as

$$p''' = \frac{A(x', x'')^{3/2}}{6\sqrt{\pi}} - s'''_o - s'''_r - l'''_e, \tag{11}$$

where

$$A(x', x'') = (1 - e_{coag}(x', x'')) \left(a_e(x')^{3/2} + a_e(x'')^{3/2} \right)^{2/3} + e_{coag}(x', x'')(a_e(x') + a_e(x'')).$$

Since $a + b \geqslant (a^{3/2} + b^{3/2})^{2/3}$, one obtains

$$\frac{A(x', x'')^{\frac{3}{2}}}{6\sqrt{\pi}} \geqslant \frac{a_e(x')^{\frac{3}{2}}}{6\sqrt{\pi}} + \frac{a_e(x')^{\frac{3}{2}}}{6\sqrt{\pi}} = s'_o + s'_r + l'_e + p' + s''_o + s''_r + l''_e + p'' \geqslant s'''_o + s'''_r + l'_e + l''_e + l'_i + l''_i = s'''_o + s'''_r + l'''_e + l'''_i$$

so that the definition (11) is consistent with the condition $p''' \geqslant l'''_i$ (cf. (1)). Moreover, (11) implies that the external surface area of the new particle satisfies (cf. (2) and (5))

$$a_e(x''') = A(x', x'').$$

2.2.2. Compaction transformation

During the collision event particles undergo compaction,

$$x \to \hat{x} = (\hat{s_o}, \hat{s_r}, \hat{l_e}, \hat{l_i}, \hat{p}) =: \hat{T}(x),$$

leading to a reduction of the pore volume. The porosity change is described by (cf. (4))

$$\Delta\varepsilon(x) = \begin{cases} k_{porred} U_{col} (\varepsilon(x) - \varepsilon_{min}), & \text{if } k_{porred} U_{col} \leqslant 1 \text{ and } \varepsilon(x) \geqslant \varepsilon_{min}, \\ 0, & \text{otherwise}, \end{cases}$$

with input parameters k_{porred} (rate constant of porosity reduction), U_{col} (collision velocity) and ε_{min} (minimum porosity, for which compaction takes place). Note that

$$\Delta\varepsilon(x) > 0 \Rightarrow \varepsilon(x) - \Delta\varepsilon(x) \geqslant \varepsilon_{min}.$$

Two scenarios are considered, depending on the critical porosity for fully saturated pores ($l_i = p$),

$$\varepsilon_{crit}(x) = \frac{l_i}{s_o + s_r + l_e + l_i}. \tag{12}$$

Case (i): If

$$\varepsilon(x) - \Delta\varepsilon(x) > \varepsilon_{crit}(x), \tag{13}$$

then the amount of external liquid remains unchanged. The components of the compacted particle are computed as

$$\widehat{s_o} = s_o, \quad \widehat{s_r} = s_r, \quad \widehat{l_e} = l_e, \quad \widehat{l_i} = l_i \tag{14}$$

and

$$\hat{p} = \frac{\varepsilon(x) - \Delta\varepsilon(x)}{1 - \varepsilon(x) + \Delta\varepsilon(x)}(s_o + s_r + l_e). \tag{15}$$

It follows from (14) and (15) that

$$v(\hat{x}) = s_o + s_r + l_e + \frac{\varepsilon(x) - \Delta\varepsilon(x)}{1 - [\varepsilon(x) - \Delta\varepsilon(x)]}(s_o + s_r + l_e) = \frac{1}{1 - [\varepsilon(x) - \Delta\varepsilon(x)]}(s_o + s_r + l_e)$$

and

$$\varepsilon(\hat{x}) = \frac{\hat{p}}{v(\hat{x})} = \varepsilon(x) - \Delta\varepsilon(x).$$

Note that the function $\frac{u}{1-u}$ is increasing for $u \in [0,1)$. Using (12), (13) and (15), one obtains (cf. (1))

$$\hat{p} \geqslant \frac{\varepsilon_{crit}(x)}{1 - \varepsilon_{crit}(x)}(s_o + s_r + l_e) = l_i = \widehat{l_i}.$$

Case (ii): If

$$\varepsilon(x) - \Delta\varepsilon(x) \leqslant \varepsilon_{crit}(x)$$

then internal liquid is squeezed onto the particle surface. The components of the compacted particle are computed as

$$\widehat{s_o} = s_o, \quad \widehat{s_r} = s_r, \quad \widehat{l_e} = l_e + l_i - \hat{p}, \quad \widehat{l_i} = \hat{p} \tag{16}$$

and

$$\hat{p} = [\varepsilon(x) - \Delta\varepsilon(x)](s_o + s_r + l_e + l_i). \tag{17}$$

It follows from (16) and (17) that

$$v(\hat{x}) = s_o + s_r + l_e + l_i - \hat{p} + \hat{p}$$

and

$$\varepsilon(\hat{x}) = \frac{\hat{p}}{v(\hat{x})} = \varepsilon(x) - \Delta\varepsilon(x).$$

Note that

$$\varepsilon_{crit}(\hat{x}) = \frac{\widehat{l_i}}{\widehat{s_o} + \widehat{s_r} + \widehat{l_e} + \widehat{l_i}} = \frac{\widehat{p}}{s_o + s_r + l_e + l_i} = \varepsilon(x) - \Delta\varepsilon(x) = \varepsilon(\hat{x}).$$

2.3. Breakage

Breakage events are characterised by the breakage frequency and the breakage transformation.

2.3.1. Breakage frequency

We consider a (parent) particle with properties x. The breakage frequency takes the form

$$g(x) = \begin{cases} \hat{k}_{att} U_{imp}^2 [\varepsilon(x)\Psi(x) + \chi(x)] v(x), & \text{if } v(x) \geqslant v_{parent,\,min}, \\ 0, & \text{otherwise} \end{cases} \tag{18}$$

with input parameters $\hat{k}_{att}$ (attrition rate constant) and U_{imp} (impact velocity, which is allowed to depend on process conditions such as the impeller speed). The quantity $v_{parent,min}$ will be defined in (23). The breakage frequency (18) includes the functions

$$\chi(x) = \frac{l_e}{v(x)} \tag{19}$$

and

$$\Psi(x) = 1 - \min\left(\frac{s_r/(s_o + s_r + p)}{s_r^*}, 1\right). \tag{20}$$

The function Ψ accounts for the solidification of the particles, with the input parameter s_r^* (dimensionless critical amount of reacted solid so that the particle core does not break).

2.3.2. Breakage transformation

The breakage transformation determines which particles are formed when a particle with properties x breaks. In the current model, particle breakage yields an "abraded parent particle" x' and a "daughter particle" x''.

The prediction of particle breakage is not fully understood yet [35]. For comminution processes, functions such as the Rosin–Rammler and Gaudin–Schuhmann distributions with two empirical parameters are widely used to describe measured particle size distributions. However, it has also been established that there is a lower particle size limit that can be achieved through breakage for a given energy input [36]. In addition, the daughter size distribution must have an upper limit. This can be modelled either by truncating an unbounded distribution [37] or by using a bounded distribution as is done in the current framework, but the consequences of this choice have not been investigated yet.

In order to define the volume of the daughter particle, a random quantity

$$v_{\mathrm{frag}}(x,\theta) = v_{\mathrm{frag,\,min}} + \theta[v_{\max} v(x) - v_{\mathrm{frag,\,min}}] \tag{21}$$

is introduced, where $\theta \in [0,1]$ is randomly chosen according to the probability density

$$f_{\mathrm{att}}(\theta) = \frac{1}{B(a,b)}\theta^{a-1}(1-\theta)^{b-1}$$

with

$$B(a,b) = \int_0^1 \theta^{a-1}(1-\theta)^{b-1}\mathrm{d}\theta \quad \text{for some } a,b \geqslant 1.$$

The quantity (21) is located on the interval

$$\left[v_{\mathrm{frag,\,min}}, v_{\max} v(x)\right].$$

It is assumed that

$$v_{\max} v(x) \geqslant v_{\mathrm{min,max}} v_{\mathrm{frag,\,min}}. \tag{22}$$

The parameter $v_{\mathrm{frag,min}}$ characterises the minimum fragment size, while $v_{\mathrm{min,max}} \geqslant 1$ provides a lower bound for the ratio of the volumes of the biggest and smallest possible fragments. The input parameter $v_{\max} \leqslant 0.5$ defines the maximum fraction of the parent particle that can break off. This quantity characterises whether fragmentation or attrition is more likely in the system. In granulation two kinds of breakage pattern can be observed, the first one being 'fragmentation'. As such, the fragments resulting from the breakage with a fragmentation pattern are rather big (something like order of magnitude compared to parent particle), whereas attrition leaves the parent particle nearly unchanged and fairly small fragments are generated. Inequality (22) gives a definition of the smallest parent particle that can be broken (cf. (18)),

$$v_{\mathrm{parent,\,min}} = \frac{v_{\mathrm{min,max}}}{v_{\max}} v_{\mathrm{frag,\,min}}. \tag{23}$$

The compositions of the newly formed fragment x'' and the abraded parent particle x' depend on the composition of the parent particle x. In the case

$$p > 0, \tag{24}$$

we define

$$s_o'' = s_o \frac{v_{\mathrm{frag}}(x,\theta)}{v(x)}, \quad s_r'' = s_r \frac{v_{\mathrm{frag}}(x,\theta)}{v(x)},$$
$$l_e'' = l_e \frac{v_{\mathrm{frag}}(x,\theta)}{v(x)}, \quad l_i'' = l_i \frac{v_{\mathrm{frag}}(x,\theta)}{v(x)}, \quad p'' = p \frac{v_{\mathrm{frag}}(x,\theta)}{v(x)},$$

so that the composition of the daughter particle is the same as for the parent particle and

$$v(x'') = v_{\mathrm{frag}}(x,\theta).$$

If the parent particle is non-porous, i.e.,

$$p = 0, \tag{25}$$

then the particle can either be a "real" particle with a completely solid core which is covered by external liquid or the particle can be a droplet ($v = l_e$). The composition of the daughter particle x'' is defined as

$$s_o'' = 0, \quad s_r'' = 0, \quad l_e'' = \min(v_{\mathrm{frag}}(x,\theta), l_e), \quad l_i'' = 0, \quad p'' = 0.$$

Note that breakage of non-porous particles without external liquid is not allowed (cf. (18)–(20)) so that

$$0 < v(x'') \leqslant v_{\mathrm{frag}}(x,\theta).$$

In both cases (24) and (25), the components of the abraded parent particle are defined as

$$s'_{\mathrm{o}} = s_{\mathrm{o}} - s''_{\mathrm{o}}, \quad s'_{\mathrm{r}} = s_{\mathrm{r}} - s''_{\mathrm{r}},$$
$$l'_{\mathrm{e}} = l_{\mathrm{e}} - l''_{\mathrm{e}}, \quad l'_{\mathrm{i}} = l_{\mathrm{i}} - l''_{\mathrm{i}}, \quad p' = p - p''.$$

2.4. Processes within a particle

Between jump events particles move according to a system of ordinary differential equations

$$\frac{\mathrm{d}}{\mathrm{d}t}(t) = D_{\mathrm{reac}}(x(t)) + D_{\mathrm{pen}}(x(t)),$$

where the term D_{reac} describes the chemical reaction in a particle and the term D_{pen} corresponds to the penetration process.

2.4.1. Chemical reaction

The chemical reaction in a particle is dependent on the rate constants $k_{\mathrm{reac,e}}$ and $k_{\mathrm{reac,i}}$ as well as on the surface areas a_{e} and a_{i}. The two contributions are computed as (reaction on external/internal surface)

$$r_{\mathrm{reac,e}}(x) = \begin{cases} k_{\mathrm{reac,e}} a_{\mathrm{e}}(x) \frac{l_{\mathrm{e}}}{l_{\mathrm{e}}+s_{\mathrm{r}}}, & \text{if } s_{\mathrm{o}} > 0 \text{ and } l_{\mathrm{e}} > 0, \\ 0, & \text{otherwise}, \end{cases}$$
$$r_{\mathrm{reac,i}}(x) = \begin{cases} k_{\mathrm{reac,i}} a_{\mathrm{i}}(x) \frac{l_{\mathrm{i}}}{l_{\mathrm{i}}+s_{\mathrm{r}}}, & \text{if } s_{\mathrm{o}} > 0 \text{ and } l_{\mathrm{i}} > 0, \\ 0, & \text{otherwise}. \end{cases} \tag{26}$$

With the assumption (3) the derivatives of each particle component are given by

$$\frac{\mathrm{d}s_{\mathrm{o}}}{\mathrm{d}t} = 0, \quad \frac{\mathrm{d}s_{\mathrm{r}}}{\mathrm{d}t} = r_{\mathrm{reac,e}}(x) + r_{\mathrm{reac,i}}(x),$$
$$\frac{\mathrm{d}l_{\mathrm{e}}}{\mathrm{d}t} = -r_{\mathrm{reac,e}}(x), \quad \frac{\mathrm{d}l_{\mathrm{i}}}{\mathrm{d}t} = -r_{\mathrm{reac,i}}(x), \quad \frac{\mathrm{d}p}{\mathrm{d}t} = -r_{\mathrm{reac,i}}(x).$$

2.4.2. Penetration

The penetration rate depends on the rate constant $\hat{k}_{\mathrm{pen}}$ and the liquid viscosity η and equates as

$$r_{\mathrm{pen}}(x) = \hat{k}_{\mathrm{pen}} \eta^{-1/2} l_{\mathrm{e}}(p - l_{\mathrm{i}}). \tag{27}$$

The derivatives in the single components are given by

$$\frac{\mathrm{d}s_{\mathrm{o}}}{\mathrm{d}t} = 0, \quad \frac{\mathrm{d}s_{\mathrm{r}}}{\mathrm{d}t} = 0,$$
$$\frac{\mathrm{d}l_{\mathrm{e}}}{\mathrm{d}t} = -r_{\mathrm{pen}}(x), \quad \frac{\mathrm{d}l_{\mathrm{i}}}{\mathrm{d}t} = r_{\mathrm{pen}}(x), \quad \frac{\mathrm{d}p}{\mathrm{d}t} = 0.$$

3. Numerical studies

Here we perform numerical studies with the Direct Simulation Monte Carlo algorithm based on the model described in the previous section. A stochastic particle system is introduced,

$$z(t) = \big(x_j(t),\ j = 1,\ldots,n(t)\big), \quad t \geqslant 0. \tag{28}$$

This system depends on a parameter N that controls the number of numerical particles. The sequence of random processes (28) approximates (as $N \to \infty$) the particle density $f(t,x)$,

$$\frac{1}{V_N} \sum_{j=1}^{n(t)} \delta_{x_j(t)}(\mathrm{d}x) \sim f(t,x)\mathrm{d}x. \tag{29}$$

The normalisation parameter V_N is such that

$$\frac{n(0)}{V_N} = \int_X f_0(x)\mathrm{d}x,$$

where f_0 is the initial particle density.

3.1. Algorithmic issues

Given a state $z = (x_1, \ldots, x_n)$, the waiting time τ for the jump process (28) is generated from

$$\mathrm{Prob}\{\tau \geqslant s\} = \exp(-\rho_{\mathrm{total}}(z)s), \quad s \geqslant 0,$$

with

$$\rho_{\mathrm{total}}(z) = \rho_{\mathrm{inc}}(z) + \rho_{\mathrm{coag}}(z) + \rho_{\mathrm{breakage}}(z).$$

The waiting time parameter for the addition of liquid is (cf. (7))

$$\rho_{\mathrm{inc}}(z) = \frac{\dot{V}_l}{V_{\mathrm{reactor}}} \frac{V_N}{\overline{V}_{\mathrm{droplet}}}. \tag{30}$$

The waiting time parameter for collisions is (cf. (8))

$$\rho_{\mathrm{coag}}(z) = \widehat{K}_0 n_{\mathrm{impeller}} \frac{n(n-1)}{2V_N}.$$

The waiting time parameter for breakage is (cf. (18))

$$\rho_{\mathrm{breakage}}(z) = \sum_{j=1}^{n} g(x_j). \tag{31}$$

At time τ, a jump mechanism is chosen according to the probabilities

$$\frac{\rho_{\mathrm{inc}}(z)}{\rho_{\mathrm{total}}(z)}, \quad \frac{\rho_{\mathrm{coag}}(z)}{\rho_{\mathrm{total}}(z)}, \quad \frac{\rho_{\mathrm{breakage}}(z)}{\rho_{\mathrm{total}}(z)},$$

leading either to the addition of a droplet, to the collision of two particles, or to the breakage of one particle. The indices of colliding particles are chosen uniformly. The index i of the particle to break is chosen according to the probabilities $g(x_i)/\rho_{\mathrm{breakage}}(z)$ (cf. (31)).

The number of particles is kept in a prescribed region by applying particle doubling and random reduction. In this study we use

$$n(0) = 0.75N \quad \text{and} \quad n(t) \in [0.375N, N] \quad \forall t \geqslant 0. \tag{32}$$

The Linear Process Deferment Algorithm [38], with a constant volume approach, is employed, where the processes within a particle are the deferred processes. The deferred processes are updated whenever a particle is involved in a collision or breakage event. In the present test case this happens about 20 times per second.

The additional error caused by these algorithmic ingredients is not significant in the present setup of the test case, so that no further details are discussed.

3.2. Confidence intervals

For each of the system properties, such as the mean number of particles per unit volume or the mean particle porosity, we study the influence of the parameter N on the convergence of the algorithm. Those macroscopic properties of the system are expressed as random variables $\xi^{(N)}(t)$ depending on time t. The empirical mean is

$$\eta_1^{(N,L)}(t) = \frac{1}{L} \sum_{l=1}^{L} \xi^{(N,l)}(t)$$

and the empirical variance is

$$\eta_2^{(N,L)}(t) = \frac{1}{L} \sum_{l=1}^{L} \xi^{(N,l)}(t)^2 - \eta_1^{(N,L)}(t)^2,$$

where L is the number of independent runs of the simulation and $\xi^{(N,l)}(t)$ denotes the value of $\xi^{(N)}(t)$ during the run l. Confidence intervals are constructed as

$$\eta_1^{(N,L)}(t) \pm a_p \sqrt{\frac{\eta_2^{(N,L)}(t)}{L}}.$$

These intervals contain the expectation of $\xi^{(N)}(t)$ with probability p. The value a_p is the solution of the equation

$$p = \sqrt{2/\pi} \int_0^{a_p} \exp(-t^2/2)\mathrm{d}t = \mathrm{erf}(a_p/\sqrt{2})$$

and can be obtained from tables for the error function. In our calculation we use $a_p = 1.64$, which corresponds to $p \simeq 0.9$.

The error is measured as

$$e^{(N,L)}(t) = \left|\eta_1^{(N,L)}(t) - \zeta(t)\right|.$$

It contains both the systematic and the statistical error. The function $\zeta(t)$ is an approximation for the true value, which is obtained from a "master calculation" with a very large number of particles. An average error is computed as

$$\bar{e}(N,L) = \frac{1}{I}\sum_{i=1}^{I} e^{(N,L)}(t_i), \tag{33}$$

where I is the number of observation points.

3.3. Approximation results

The model provides an estimate for the particle density f (cf. (29)). From this, practically relevant properties of the particle ensemble and subsets of it can be derived. Ensemble in this context means the population of all entities.

In our calculation the "true" solution is obtained from a run with $N = 524{,}288$ (cf. (32)) and $L = 8$ repetitions. Otherwise, the product $N \times L = 524{,}288$ is kept constant so that the width of the confidence bands is roughly the same for all curves. The observed order of convergence of the systematic error is $1/N$ (indicated by the solid lines in the corresponding figures). The values of the model parameters used in the test case are summarised in Table B.1 in Appendix A.

3.3.1. Ensemble properties

The examination of a batch of (numerical) particles allows for the deduction of various characteristics of the ensemble.

3.3.1.1. Number of particles per unit volume. The number of particles per unit volume, i.e., the zeroth moment

$$m_0(t) = \frac{n(t)}{V_N}, \tag{34}$$

is the simplest property of the particle ensemble. This quantity is governed by the interplay of the different processes, with inception/inflow and particle breakage leading to an increase, and coalescence leading to a decrease of the number of particles. Its dependence on the parameters N (cf. (32)) and L (number of repetitions) is shown in Fig. 1, while the error (33) is displayed in Fig. 2.

3.3.1.2. Volume of particles per unit volume. From the composition of each particle, the individual particle volume (2) can be computed. The summation over all particles leads to the first moment

$$m_1(t) = \frac{1}{V_N}\sum_{i=1}^{n(t)} v(x_i(t)), \tag{35}$$

which is the fraction of the control volume (i.e., apparatus) taken up by the particulate matter. The dependence of this quantity on the parameters N and L is shown in Fig. 3. Note that quantity (35) is less than the apparent volume fraction of the packed particle ensemble due to the interstitial voidage between the particles.

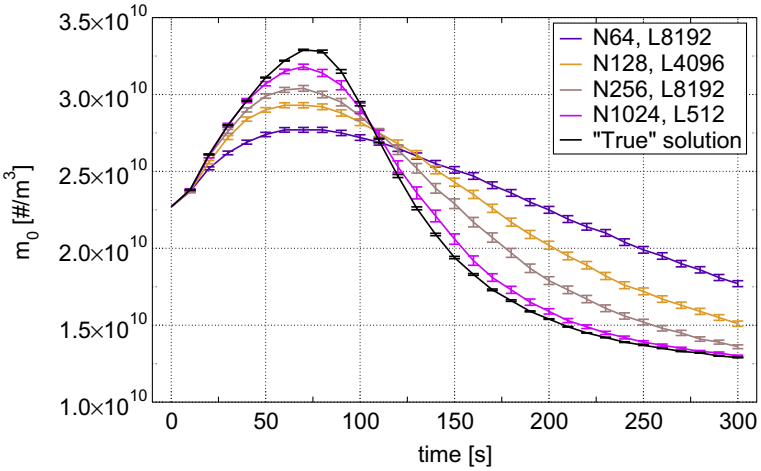

Fig. 1. Number of particles per unit volume (34).

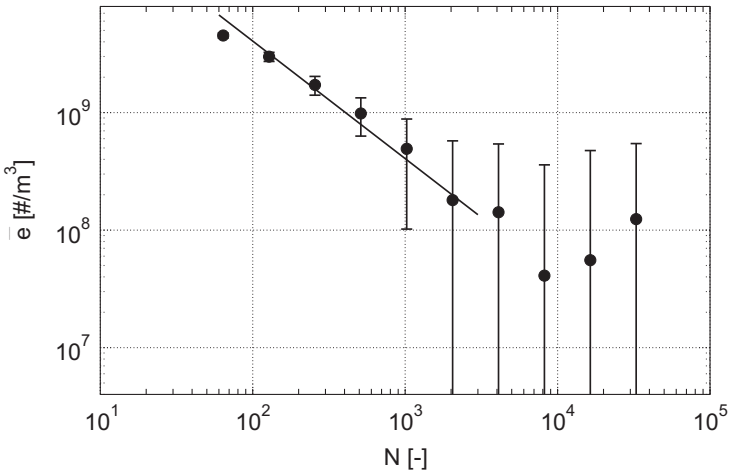

Fig. 2. Error in quantity (34) as function of N (cf. (32)).

3.3.1.3. Mean particle porosity. Apart from solids and liquids, the pore volume of each particle is tracked in the multidimensional model, allowing for the computation of the particle porosity. This property is often of importance for particulate matter and crucial for the dissolution/disintegration of granules, e.g. pharmaceuticals, fertilizer or detergents. A number averaged porosity shall be defined by

$$\varepsilon_{0,\mathrm{m}}(t) = \frac{1}{n(t)} \sum_{i=1}^{n(t)} \varepsilon(x_i(t)). \tag{36}$$

The dependence of this quantity on the parameters N and L is shown in Fig. 4.

3.3.2. Sieve class properties

For the use of the granules in a specific application, e.g. as detergent, certain characteristics need to be met. A common classification of the particles is the one by size. This means, the product has to pass a set of screens, and granules being too small (undersize) or too big (oversize) are removed. In order to mimic such sieving/screening process, the computational ensemble is split according to the particle sizes into classes (that would result from a screening process). The "sieves" are chosen from standard sieve series and have mesh sizes of 150, 300, 600, and 1200 μm, leading to three classes (150 and 1200 μm happened to encompass the diameters of all existing particles).

3.3.2.1. Mass fraction in sieve classes. For each of the sieve classes we define the mass fraction of the particular sieve cut in the particle ensemble,

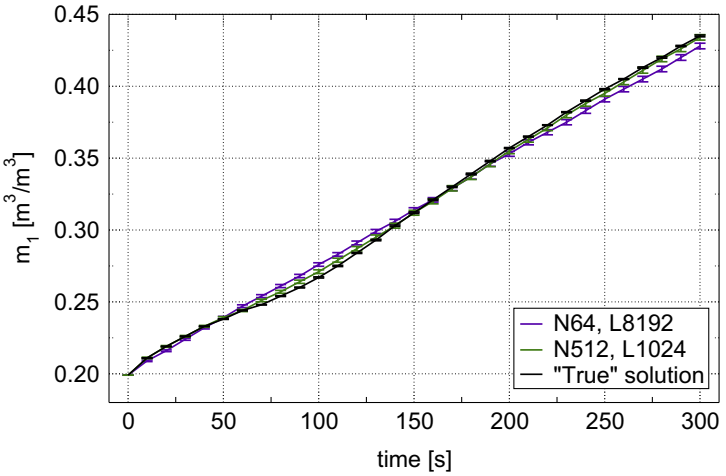

Fig. 3. Volume of particles per unit volume (35).

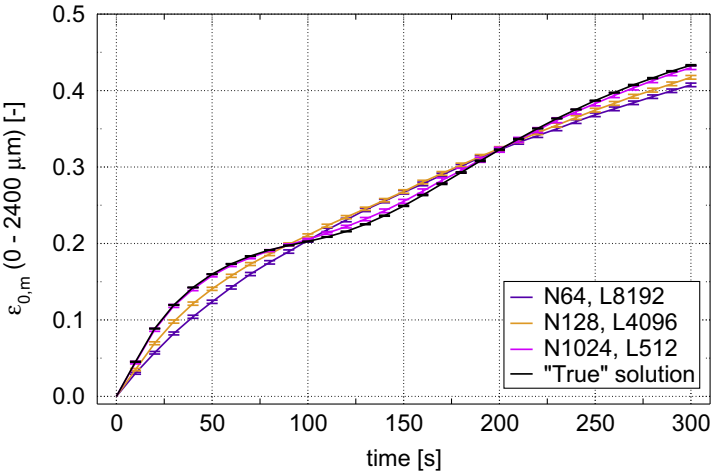

Fig. 4. Number averaged porosity (36).

$$q_{3,k}(l_{\mathrm{low},k}, l_{\mathrm{up},k}) = \frac{m_k(l_{\mathrm{low},k}, l_{\mathrm{up},k})}{m_{\mathrm{total}}}, \tag{37}$$

where k is the number of the class, $l_{\mathrm{low},k}$ and $l_{\mathrm{up},k}$ are the lower and upper boundary of the class, m_k is the mass of the particles in the class and m_{total} is the mass of the entire ensemble. The dependence of the quantities (37) on the parameters N (cf. (32)) and L (number of repetitions) is shown in Figs. 5 (150–300 µm), 7 (300–600 µm) and Fig. 9 (600–1200 µm). The corresponding errors (33) are displayed in Figs. 6, 8 and 10.

3.3.2.2. Mean particle porosity in sieve classes. Once the granules are classified, it is not only of interest how much material belongs to each size class, but also which properties the particles in each class have. One of them is the porosity of the particles, and distinctive differences can be observed for the particles of the different size classes. The dependence of the quantities (36) in each class on the parameters N and L is shown in Figs. 11, 13 and 15. The corresponding errors (33) are displayed in Figs. 12, 14 and 16.

3.4. Efficiency issues

The main focus of the numerical experiments was studying the convergence of the measured quantities with respect to the parameter N (cf. (32)). Confidence bands turned out to be sufficiently narrow to illustrate this behaviour and even to indicate the order of convergence. However, the calculations were rather time-consuming so that increasing the efficiency is a challenging task. In the context of stochastic particle methods an appropriate tool is variance reduction, i.e., modifying the

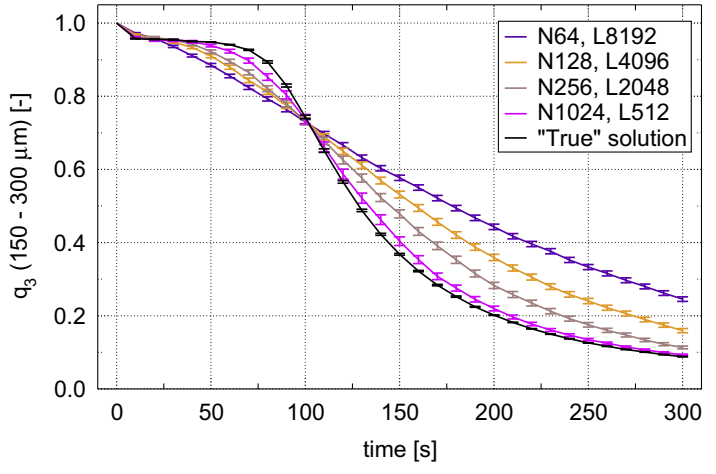

Fig. 5. Mass fraction (37) of sieve class 150–300 µm.

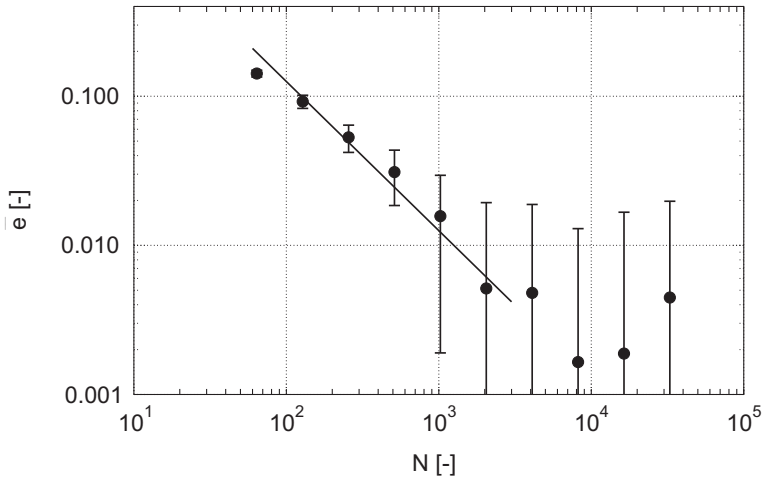

Fig. 6. Error in quantity (37) for sieve class 150–300 μm as function of *N*.

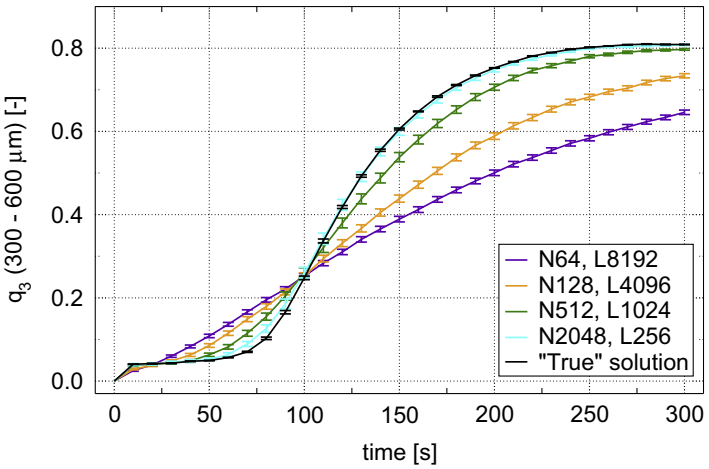

Fig. 7. Mass fraction (37) of sieve class 300–600 μm.

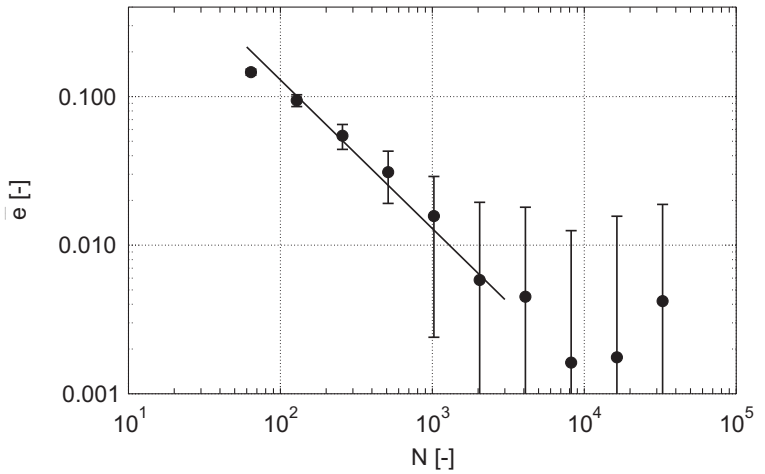

Fig. 8. Error in quantity (37) for sieve class 300–600 μm as function of *N*.

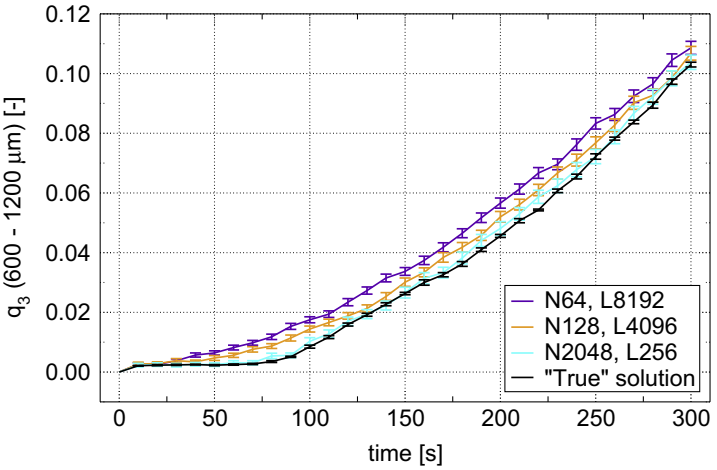

Fig. 9. Mass fraction (37) of sieve class 600–1200 µm.

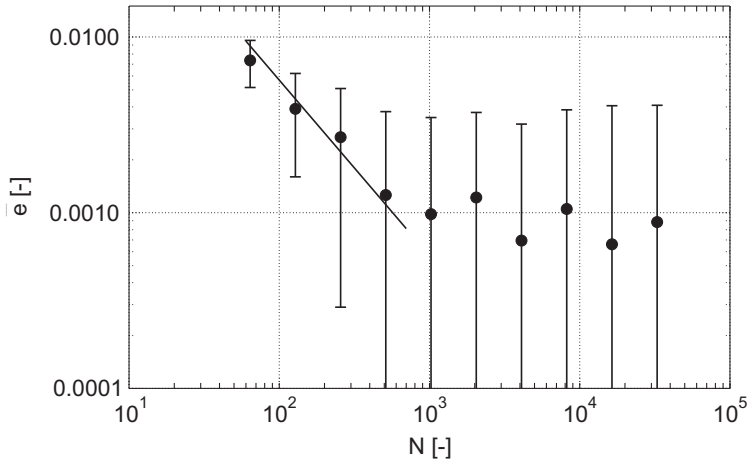

Fig. 10. Error in quantity (37) for sieve class 600–1200 µm as function of N.

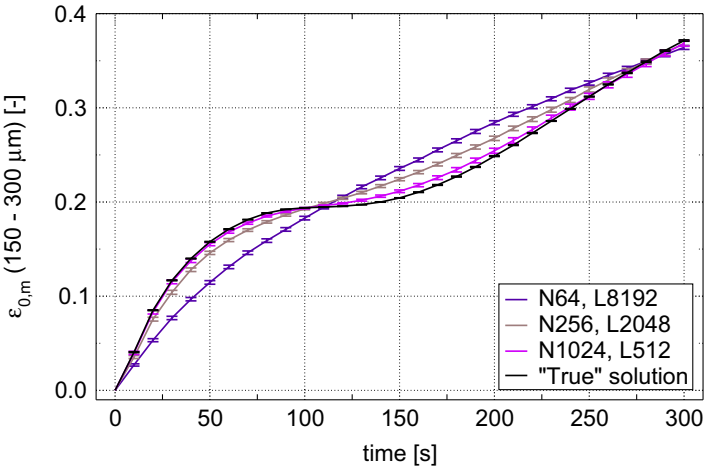

Fig. 11. Number averaged porosity (36) in sieve class 150–300 µm.

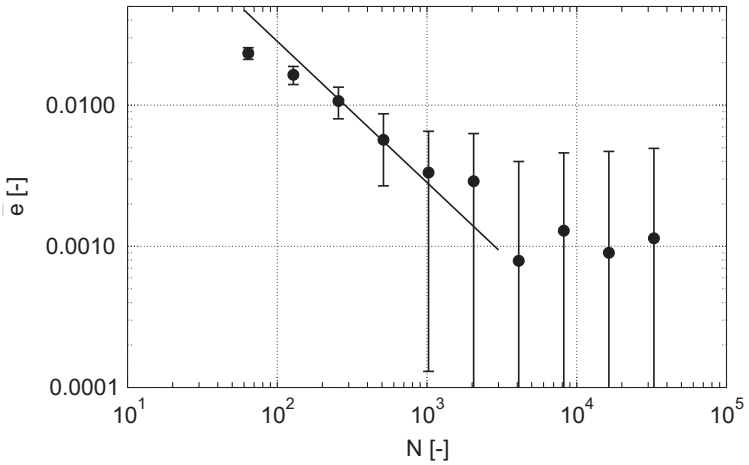

Fig. 12. Error in quantity (36) for sieve class 150–300 μm as function of *N*.

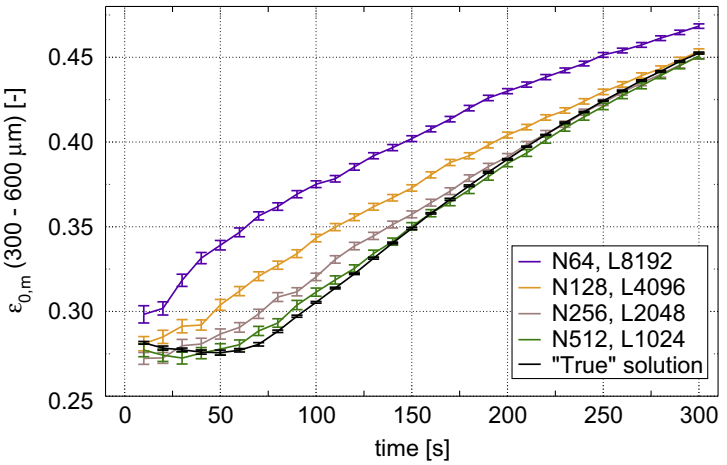

Fig. 13. Number averaged porosity (36) in sieve class 300–600 μm.

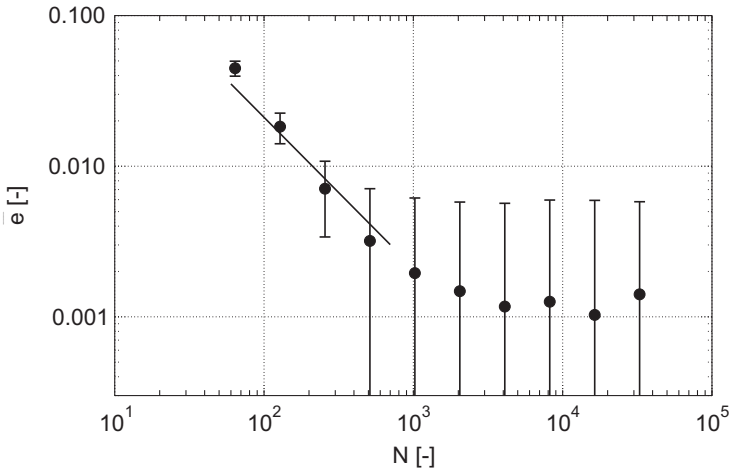

Fig. 14. Error in quantity (36) for sieve class 300–600 μm as function of *N*.

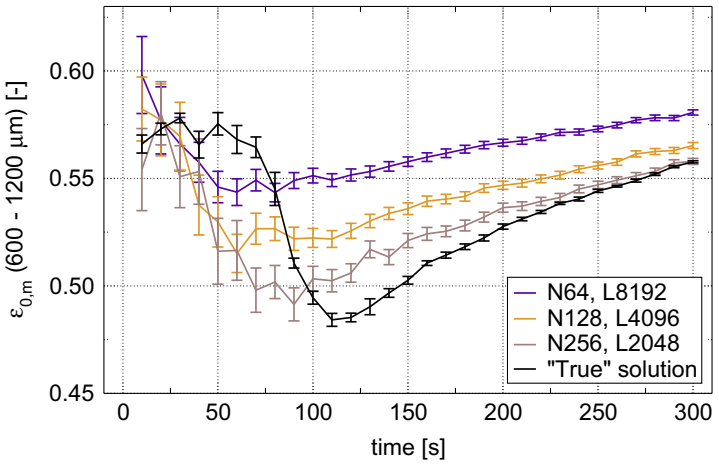

Fig. 15. Number averaged porosity (36) in sieve class 600–1200 µm.

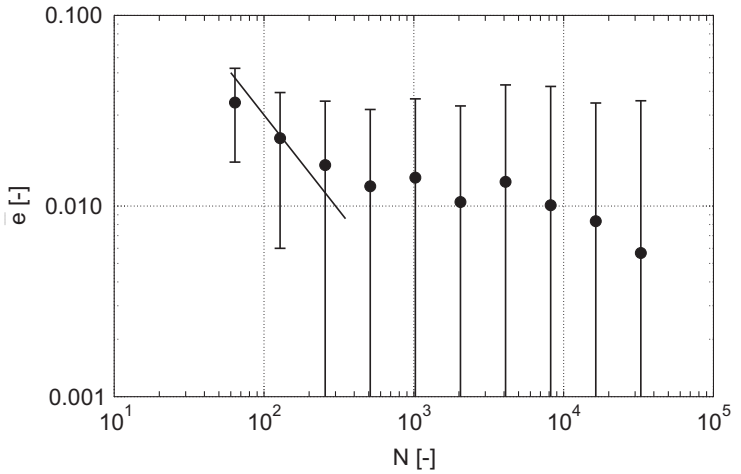

Fig. 16. Error in quantity (36) for sieve class 600–1200 µm as function of N.

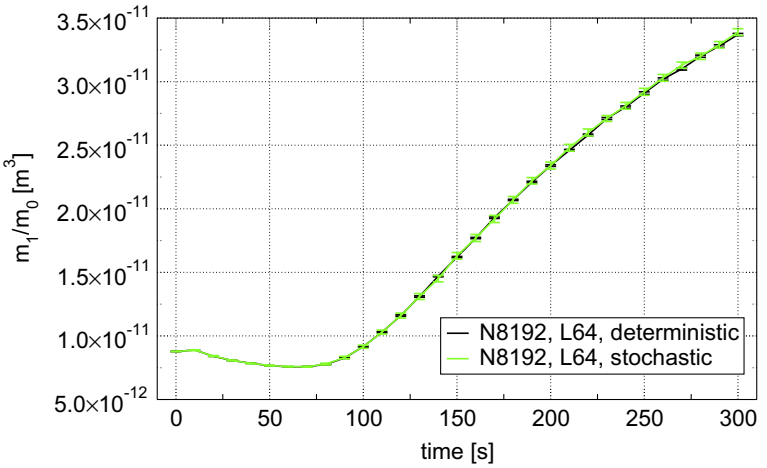

Fig. 17. Mean volume (38) for deterministic and stochastic liquid addition.

algorithm in such a way that the mean quantities are similar, but the stochastic fluctuations are smaller. This allows to get the same approximations by producing fewer trajectories of the particle ensemble. We have not really addressed the variance reduction problem so far, but the following observations should be mentioned in this context.

3.4.1. Stochastic versus deterministic liquid addition

The addition of droplets to the particle ensemble is performed as a Markov jump process (cf. Section 3.1). Alternatively, the droplets can be added after a predetermined time step $1/\rho_{\mathrm{inc}}(z)$ (cf. (30)), which is a function of the process conditions (mean droplet size, liquid flow rate) and of the numerical parameter N.

With this deterministic droplet addition, it has been observed that the fluctuations in the measured quantities are reduced compared to the case when the droplets are added in a stochastic manner. For example, the plot of the mean volume

$$\bar{v}(t) = \frac{m_1(t)}{m_0(t)} = \frac{1}{n(t)} \sum_{i=1}^{n(t)} v(x_i(t)) \tag{38}$$

in Fig. 17 shows that the model response is approximately the same. However, the uncertainty is on average about three times higher for stochastic liquid addition compared to the deterministic version. The runtimes for both simulations were roughly the same (about 43,000 s $\simeq$ 11.5 h on AMD Opteron™ Processor 252, 2.6 GHz).

4. Conclusions

A numerical study of the solution of a multidimensional population balance model for wet granulation with a stochastic algorithm has been performed. The stochastic particle model was described in detail, with each particle consisting of two kinds of solid, two kinds of liquid and pores. Various transformations are part of the model, for instance coalescence, compaction and breakage of the particles. Due to the complexity of the model the weak form of the kinetic equation which corresponds to the stochastic process has been stated. A convergence study of the stochastic algorithm was performed with respect to the number of numerical particles.

Fast convergence of order $1/N$ was achieved for properties of the whole ensemble, such as the number of particles and the average particle porosity. For example, with 2000 numerical particles the error in the average particle porosity was less than 1%.

In order to mimic a granules production, the numerical particle ensemble was divided into practically relevant size classes. The mass fraction and the particle porosity of these size classes as function of the number of numerical particles were studied. The order of the convergence remained the same, however larger number of numerical particles are required to achieve small errors.

Finally, a stochastic and a deterministic model of liquid addition were studied. The deterministic addition of droplets proofed to reduce the fluctuations in the observed quantities.

For the first time a relationship between numerical error and approximation parameter for a complex multivariate population balance has been presented. Thus the current study serves as a benchmark for future algorithm improvements and new possibly deterministic algorithms. The information is also useful to construct surrogate models which are needed to solve the inverse problem, i.e., estimate the parameters in the model for a given set of experimental observations.

Acknowledgments

The authors thank the EPRSC (Grant EP/E01772X/1), Churchill College and the Weierstrass Institute for Applied Analysis and Stochastics (MK) for financial support.

Appendix A. The kinetic equation

Here we introduce the kinetic equation satisfied by the particle density $f(t,x)$. This equation might be of interest for future analytical studies of the model, or for deriving alternative numerical procedures.

Due to the complexity of the stochastic process considered in this paper, it is not possible to provide a kinetic equation for the particle density in the common strong form. Instead, a weak form of the equation is given, where the solution is integrated with respect to appropriate test functions. Nonlinear kinetic equations with an inflow term and rather general interactions were studied in [39, Theorem 2.3]. A particular nonlinear kinetic equation with a gradient term was considered in [40, Section 2.2.1]. According to these results, the temporal evolution of the particle density $f(x,t)$ for a batch process with no outflow is characterised by the equation

$$\frac{\mathrm{d}}{\mathrm{d}t}\int_X \varphi(x) f(t,x)\mathrm{d}x = \int_X [(D(x),\nabla_x)\varphi(x)] f(t,x)\mathrm{d}x + \int_X \varphi(x) f^{\mathrm{in}}(x)\mathrm{d}x + \int_X \left[\int_E [\langle\varphi,\xi\rangle - \varphi(x)] q_1(x,\mathrm{d}\xi)\right] f(t,x)\mathrm{d}x + \int_X \int_X \left[\int_E [\langle\varphi,\xi\rangle - \varphi(x) - \varphi(y)] q_2(x,y,\mathrm{d}\xi)\right] f(t,x) f(t,y)\mathrm{d}x\,\mathrm{d}y,$$

where the test functions φ should be differentiable and have compact support. To keep terms short and the structure of the equation transparent, we use kernels q_1, q_2 and the notations

$$\langle\varphi,\xi\rangle = \sum_{i=1}^{k} \varphi(\xi_i), \quad \xi \in E := X \cup X^2.$$

The kernel q_1 describes the jumps involving one particle (e.g., fragmentation), while the kernel q_2 determines the binary interactions (e.g., collision).

Table B.1
Values of model parameters.

Parameter	Unit	Value
Starting material		
Solid particles		
s_o	m^3	$8.78 \cdot 10^{-12}$
ρ_{s_o}	kg/m^3	2509
Liquid droplets		
$V_{droplet} = l_e$	m^3	$6.54 \cdot 10^{-11}$
η_l	Pa s	$23 \cdot 10^{-3}$
ρ_{l_e}	kg/m^3	1025
Mixer-granulator operating parameters		
$\dot{V}_l$	m^3/s	$1.084 \cdot 10^{-6}$
$n_{impeller}$	s^{-1}	3
U_{col}	m/s	0.13
U_{imp}	m/s	1.19
Breakage		
$\hat{k}_{att}$	$s\ m^{-5}$	$8.0 \cdot 10^{10}$
s_r^*	–	$1.0 \cdot 10^{20}$
a	–	5.0
b	–	2.0
$v_{frag,min}$	m^3	$4.1888 \cdot 10^{-12}$
v_{max}	–	0.5
$v_{min,max}$	–	1.1
Chemical reaction		
C	–	15
$k_{reac,e}$	m/s	$1.0 \cdot 10^{-8}$
$k_{reac,i}$	m/s	$1.0 \cdot 10^{-8}$
Coalescence		
e_{s_o}	–	1
e_{s_r}	–	1
e_{l_i}	–	0
h_a	m	$1.0 \cdot 10^{-6}$
$\widehat{K}_0$	m^3	$1.0 \cdot 10^{-9}$
Compaction		
k_{porred}	s/m	0.4
ε_{min}	–	0.25
Penetration		
$\hat{k}_{pen}$	$kg^{1/2}\ s^{-3/2}\ m^{-7/2}$	$1.0 \cdot 10^{10}$

For our particular model, the function f^{in} is given in (6) and (cf. (26) and (27))

$$D(x) = \begin{pmatrix} 0 \\ r_{\text{reac,e}}(x) + r_{\text{reac,i}}(x) \\ -r_{\text{reac,e}}(x) - r_{\text{pen}}(x) \\ -r_{\text{reac,i}}(x) + r_{\text{pen}}(x) \\ -r_{\text{reac,i}}(x) \end{pmatrix}.$$

Moreover, one obtains (see Section 2.3)

$$\int_E [\langle \varphi, \xi \rangle - \varphi(x)] q_1(x, \mathrm{d}\xi) = g(x) \int_0^1 f_{\text{att}}(\theta)[\varphi(x'(x,\theta)) + \varphi(x''(x,\theta)) - \varphi(x)]\mathrm{d}\theta$$

and (see Section 2.2)

$$\int_E [\langle \varphi, \xi \rangle - \varphi(x) - \varphi(y)] q_2(x, y, \mathrm{d}\xi) = \frac{1}{2} n_{\text{impeller}} \widehat{K}_0 \times \left\{ \varphi(T(x,y))\widetilde{K}(x,y) + [\varphi(\widehat{T}(x)) + \varphi(\widehat{T}(y))](1 - \widetilde{K}(x,y)) - \varphi(x) - \varphi(y) \right\}.$$

Appendix B. Values of model parameters in test case

See Table B.1.

References

[1] G.I. Tardos, M.I. Khan, P.R. Mort, Critical parameters and limiting conditions in binder granulation of fine powders, Powder Technol. 94 (1997) 245–258.
[2] P.C. Kapur, D.W. Fuerstenau, A coalescence model for granulation, I&EC Process. Design Dev. 8 (1969) 56–62.
[3] K.V.S. Sastry, Similarity size distribution of agglomerates during their growth by coalescence in granulation or green pelletization, Int. J. Miner. Process. 2 (1975) 187–203.
[4] S.M. Iveson, Limitations of one-dimensional population balance models of wet granulation processes, Powder Technol. 124 (2002) 219–229.
[5] D. Verkoeijen, G.A. Pouw, G.M.H. Meesters, B. Scarlett, Population balances for particulate processes – a volume approach, Chem. Eng. Sci. 57 (2002) 2287–2303.
[6] A. Darelius, H. Brage, A. Rasmuson, I.N. Björn, S. Folestad, A volume-based multi-dimensional population balance approach for modelling high shear granulation, Chem. Eng. Sci. 61 (2006) 2482–2493.
[7] J.A. Gantt, T. Palathra, E.P. Gatzke, Analysis of the multidimensional behavior of granulation, J. Mater. Process. Technol. 183 (2007) 140–147.
[8] J.M.-H. Poon, C.D. Immanuel, F.J. Doyle III, J.D. Litster, A three-dimensional population balance model of granulation with a mechanistic representation of the nucleation and aggregation phenomena, Chem. Eng. Sci. 63 (2008) 1315–1329.
[9] A. Braumann, M.J. Goodson, M. Kraft, P.R. Mort, Modelling and validation of granulation with heterogeneous binder dispersion and chemical reaction, Chem. Eng. Sci. 62 (2007) 4717–4728.
[10] A. Braumann, M. Kraft, P.R. Mort, Parameter estimation in a multidimensional granulation model, Powder Technol. 197 (2010) 196–210.
[11] P. Rajniak, F. Stepanek, K. Dhanasekharan, R. Fan, C. Mancinelli, R.T. Chern, A combined experimental and computational study of wet granulation in a Wurster fluid bed granulator, Powder Technol. 189 (2009) 190–201.
[12] A.A. Adetayo, J.D. Litster, S.E. Pratsinis, B.J. Ennis, Population balance modelling of drum granulation of material with wide size distribution, Powder Technol. 82 (1995) 37–49.
[13] S. Heinrich, M. Peglow, M. Ihlow, M. Henneberg, L. Mörl, Analysis of the start-up process in continuous fluidized bed spray granulation by population balance modelling, Chem. Eng. Sci. 57 (2002) 4369–4390.
[14] N.E. Balliu, I.T. Cameron, R. Newell, A comparative study of numerical methods for solving continuous population balance models for aggregation processes, Dev. Chem. Eng. Miner. Process. 12 (2004) 277–291.
[15] H.S. Tan, A.D. Salman, M.J. Hounslow, Kinetics of fluidized bed melt granulation – II: Modelling the net rate of growth, Chem. Eng. Sci. 61 (2006) 3930–3941.
[16] C.D. Immanuel, F.J. Doyle III, Solution technique for a multi-dimensional population balance model describing granulation processes, Powder Technol. 156 (2005) 213–225.
[17] J.R. van Peborgh Gooch, M.J. Hounslow, Monte Carlo simulation of size-enlargement mechanisms in crystallization, AIChE J. 42 (1996) 1864–1874.
[18] M.K. Akhtar, G.G. Lipscomb, S.E. Pratsinis, Monte Carlo simulation of particle coagulation and sintering, Aerosol Sci. Technol. 21 (1994) 83–93.
[19] M. Goodson, M. Kraft, An efficient stochastic algorithm for simulating nano-particle dynamics, J. Comput. Phys. 183 (2002) 210–232.
[20] H.-J. Schmid, S. Tejwani, C. Artelt, W. Peukert, Monte Carlo simulation of aggregate morphology for simultaneous coagulation and sintering, J. Nanopart. Res. 6 (2004) 613–626.
[21] N.M. Morgan, C.G. Wells, M.J. Goodson, M. Kraft, W. Wagner, A new numerical approach for the simulation of the growth of inorganic nanoparticles, J. Comput. Phys. 211 (2006) 638–658.
[22] M. Sander, R.H. West, M.S. Celnik, M. Kraft, A detailed model for the sintering of polydispersed nanoparticle agglomerates, Aerosol Sci. Technol. 43 (2009) 978–989.
[23] J.A. Gantt, E.P. Gatzke, A stochastic technique for multidimensional granulation modelling, AIChE J. 52 (2006) 3067–3077.
[24] K. Terrazas-Velarde, M. Peglow, E. Tsotsas, Stochastic simulation of agglomerate formation in fluidized bed spray drying: a micro-scale approach, Chem. Eng. Sci. 64 (2009) 2631–2643.
[25] D.T. Gillespie, A general method for numerically simulating the stochastic time evolution of coupled chemical reactions, J. Comput. Phys. 22 (1976) 403–434.
[26] M.A. Hsia, L.L. Tavlarides, A simulation model for homogeneous dispersions in stirred tanks, Chem. Eng. J. 20 (1980) 225–236.
[27] A. Vikhansky, M. Kraft, Modelling of a RDC using a combined CFD-population balance approach, Chem. Eng. Sci. 59 (2004) 2597–2606.
[28] D.T. Gillespie, An exact method for numerically simulating the stochastic coalescence process in a cloud, J. Atmos. Sci. 32 (1975) 1977–1989.
[29] E. Debry, B. Sportisse, B. Jourdain, A stochastic approach for the numerical simulation of the general dynamics equation for aerosols, J. Comput. Phys. 184 (2003) 649–669.
[30] M. Smith, T. Matsoukas, Constant-number Monte Carlo simulation of population balances, Chem. Eng. Sci. 53 (1998) 1777–1786.
[31] F.E. Kruis, A. Maisels, H. Fissan, Direct simulation Monte Carlo method for particle coagulation and aggregation, AIChE J. 46 (2000) 1735–1742.
[32] M. Vicanek, N.M. Ghoniem, Two-group approach to the kinetics of particle cluster aggregation, J. Comput. Phys. 101 (1992) 1–10.

[33] I.J. Laurenzi, J.D. Bartels, S.L. Diamond, A general algorithm for exact simulation of multicomponent aggregation processes, J. Comput. Phys. 177 (2002) 418–449.
[34] B.J. Ennis, G. Tardos, R. Pfeffer, A microlevel-based characterization of granulation phenomena, Powder Technol. 65 (1991) 257–272.
[35] A.D. Salman, G.K. Reynolds, M.J. Hounslow, Particle impact breakage in particulate processing, KONA 21 (2003) 88–99.
[36] L. Vogel, W. Peukert, Breakage behaviour of different materials – construction of a mastercurve for breakage probability, Powder Technol. 129 (2003) 101–110.
[37] M.J. Hounslow, J.M.K. Pearson, T. Instone, Tracer studies of high-shear granulation: II. Population balance modeling, AIChE J. 47 (2001) 1984–1999.
[38] R.I.A. Patterson, J. Singh, M. Balthasar, M. Kraft, J.R. Norris, The linear process deferment algorithm: a new technique for solving population balance equations, SIAM J. Sci. Comput. 28 (2006) 303–320.
[39] A. Eibeck, W. Wagner, Stochastic interacting particle systems and nonlinear kinetic equations, Ann. Appl. Probab. 13 (2003) 845–889.
[40] S. Rjasanow, W. Wagner, Stochastic Numerics for the Boltzmann Equation, Springer, Berlin, 2005.